

Determinants of HIV-induced brain changes in three different periods of the early clinical course: A data mining analysis



Bokai Cao^a, Xiangnan Kong^b, Casey Kettering^c, Philip Yu^a, Ann Ragin^{c,*}

^aDepartment of Computer Science, University of Illinois at Chicago, 851 S. Morgan, Chicago, IL 60607, USA

^bDepartment of Computer Science, Worcester Polytechnic Institute, 100 Institute Road, Worcester, MA 01609, USA

^cDepartment of Radiology, Feinberg School of Medicine, Northwestern University, Suite 1600, 737 N. Michigan Ave, Chicago, IL 60611, USA

ARTICLE INFO

Available online 1 August 2015

Keywords:

Acute HIV
Neuroinflammation
Cytokines
Corpus callosum
MMP-1
Data mining

ABSTRACT

To inform an understanding of brain status in HIV infection, quantitative imaging measurements were derived at structural, microstructural and macromolecular levels in three different periods of early infection and then analyzed simultaneously at each stage using data mining. Support vector machine recursive feature elimination was then used for simultaneous analysis of subject characteristics, clinical and behavioral variables, and immunologic measures in plasma and CSF to rank features associated with the most discriminating brain alterations in each period. The results indicate alterations beginning in initial infection and in all periods studied. The severity of immunosuppression in the initial virus host interaction was the most highly ranked determinant of earliest brain alterations. These results shed light on the initial brain changes induced by a neurotropic virus and their subsequent evolution. The pattern of ongoing alterations occurring during and beyond the period in which virus is suppressed in the systemic circulation supports the brain as a viral reservoir that may preclude eradication in the host. Data mining capabilities that can address high dimensionality and simultaneous analysis of disparate information sources have considerable utility for identifying mechanisms underlying onset of neurological injury and for informing new therapeutic targets.

© 2015 The Authors. Published by Elsevier Inc. This is an open access article under the CC BY-NC-ND license (<http://creativecommons.org/licenses/by-nc-nd/4.0/>).

1. Introduction

Injury to the brain is a serious complication of Human Immunodeficiency Virus (HIV). Early viral invasion of the brain is evidenced by virus in cerebrospinal fluid within only 7–10 days of transmission (Valcour, 2012a). Subsequent changes, however, are not well characterized because the infection often remains undiagnosed in the earliest stages. Additionally, to evaluate the brain in subclinical periods requires quantitative imaging which is not routinely available. This investigation used Magnetic Resonance (MR) imaging to examine the brain at structural, microstructural and macromolecular levels in three different periods of the early clinical course: Primary Infection, 4–12 months post-infection (pi) and >12–24 months pi. Duration of infection was determined by antibody non-reactivity (for Primary Infection) and assay values from a recent infection testing algorithm (Keating, 2012). Volumetric measurements were derived from high resolution neuroanatomic images for the major tissue classes with SIENAX (Smith, 2002) and for approximately fifty individual brain regions with Freesurfer

(Fischl, 2002). Diffusion Tensor Imaging (DTI) parameters, fractional anisotropy (FA) and mean diffusivity (MD), were used to quantify microstructural alterations at levels approximating cellular dimensions (Basser and Pierpaoli, 1996a). Magnetization Transfer Ratio (MTR) was used to quantify macromolecular changes (e.g. in lipids, membranes, myelin) (Wolff and Balaban, 1994). DTI and MT parameters (FA, MD and MTR) were calculated for 3D volumes of interest, including cerebral cortex, cerebral white matter, corpus callosum, caudate, putamen, thalamus and hippocampus. Data mining methods were used to analyze measurements from the multiple MRI sequences simultaneously in order to determine the most discriminating brain measures (features) in each period of HIV infection compared to normative values from age matched seronegative controls. Recursive feature selection was also used to determine factors most highly associated with a composite measure of the brain alterations identified in each period. This analysis considered subject characteristics, clinical laboratory measures (e.g. HIV RNA and complete blood count), medical history information, behavioral measures (e.g. alcohol/substance use), and immunologic measures in plasma and CSF.

2. Materials and methods

Northwestern University Institutional Review Board approved this investigation, which was conducted in compliance with U.S. federal

* Corresponding author: Tel.: +1 312 695 1628; fax: +1 312 926 5991.

E-mail addresses: caobokai@uic.edu (B. Cao), xkong@wpi.edu (X. Kong), casey.kettering@northwestern.edu (C. Kettering), psyu@uic.edu (P. Yu), ann-ragin@northwestern.edu (A. Ragin).

guidelines. Informed consent was obtained from all subjects. The study included 56 HIV (50 males, 6 females; mean age: 33.3 ± 10.1 years) and 21 seronegative control (16 males, 5 females; mean age: 31.4 ± 8.9 years) subjects. Study exclusion criteria included chronic neurological disorder, head injury, uncontrolled seizure disorder, experimental drugs or vaccination within the past 15 days, radiation or chemotherapy within prior month, mental condition involving inability to understand, chronic alcohol or drug abuse, pregnancy, opportunistic infection, cancer, medical condition (heart, liver or kidney) or MR contraindication. None of the participants had history of Kaposi's sarcoma, primary CNS lymphoma, non-CNS lymphoma or prior radiation therapy. Demographic and clinical information is presented in Table 1. HIV and seronegative groups did not differ in age, gender, racial composition or education level. Marijuana use was reported by more participants in the HIV than control group.

Blood samples were collected from all subjects; CSF was acquired from consenting HIV subjects ($n = 11$). HIV serostatus was determined by enzyme-linked immunosorbent assay and Western blot. An early infection assay (EIA) was used to assess duration of infection (Blood Systems Research Institute, San Francisco, CA). Antibody non-reactivity was used to define Primary Infection (estimated as less than 4 months pi; $n = 15$); 4–12 months pi ($n = 15$; EIA: 7.65–35.5), infected >12–24 months ($n = 26$; EIA >35.5). For the HIV group, absolute CD4 T cell counts ranged from 139 to 1282 cells/ μ L (mean: 546 ± 254.0 cells/ μ L); plasma viral load (\log_{10}) ranged from undetectable to 5.54 copies/mL (mean: 3.34 ± 1.5 copies/mL). Plasma viral load was undetectable (<50 copies/mL) in 11 of the 56 HIV subjects, including 10 suppressed on antiretroviral therapy (ART) (0–4 months pi: $n = 2$; 4–12 months pi: $n = 2$, >12–24 months pi: $n = 6$). Thirty of the HIV subjects were ART naïve and 26 had initiated treatment with subgroup distribution as follows: (0–4 months pi: 7 naïve, 8 ART), (4–12 months pi: 11 naïve, 4 ART) and (>12–24 months pi: 12 naïve; 14 ART).

2.1. Cytokine/chemokine quantification

Multiplex analyses were conducted at Blood Systems Research Institute (San Francisco). Plasma/CSF was aliquoted locally, frozen and shipped for long-term storage and for batched analysis. The high-sensitivity Milliplex kit (Millipore) was used for IL-1 β , IL-2, IL-4, IL-5, IL-6, IL-7, IL-8, IL-10, IL-12 p70, IL-13, IFN- γ , GM-CSF and TNF- α . The standard-sensitivity Milliplex Map kit (Millipore) was used for epidermal growth factor (EGF), Eotaxin, fibroblast growth factor (FGF)-2, Fractalkine, IL-1 α , IL-1R α , IL-9, IL-12 (p40), IL-15, IL-17, IP-10, monocyte chemoattractant protein (MCP)-1, MCP-3, macrophage-derived chemokine (MDC), macrophage inflammatory protein (MIP)-1 α , MIP-1 β , sIL-2R α , TNF β , and vascular endothelial growth factor (VEGF). The MMP panel

Table 1
Demographic characteristics.

	HIV (n = 56)	Control (n = 21)	p
Age (mean years \pm SD)	33.3 ± 10.1	31.4 ± 8.9	0.45
Gender (% male)	89%	76%	0.22
Race (% White)	62%	76%	0.22
Education (% college)	81%	90%	0.29
<i>Substance use (past month)</i>			
Alcohol (5 or more drinks)	7	4	0.51
Marijuana	20	3	0.04
Cocaine	3	0	0.08
Amphetamines	2	0	0.39
Glue or solvent sniffing	0	0	–
Heroin	0	0	–
Other	3	0	0.08

2 was used for MMP-1, MMP-2, MMP-7, MMP-9, MMP-10 and a singleplex was used for SDF-1. Manufacturer's protocols were followed. Serum was incubated overnight with antibody-coupled beads followed by incubation with biotinylated detection antibody, and finally, incubation with streptavidin-PE. Each sample was assayed in duplicate and cytokine standards, and controls, supplied by the manufacturer, were run on each plate. In addition, manufacturer controls and in-house controls consisting of supernatants of PBMCs stimulated with mitogen in culture are also run. Multi-analyte profiling was performed using a Luminex-100 system and data were analyzed using BioPlex 6.1 software (BioPlex). Luminex Standard Curve: A 5-PL curve fit is used to graph the 7-point standard curve. The curve for every analyte was checked for the fit of the standard data points. If there were errors or more than a 30% CV for any standard, those points were dropped. The curve fit parameter was altered if necessary depending on the number of standard points.

2.2. Flow cytometry

Whole blood was collected into ethylenediaminetetraacetic acid (EDTA) anticoagulant and assayed within 24 h. Samples were processed using a simple lyse-wash-stain-wash technique. For a given sample, sixteen 5-mL polystyrene tubes were each filled with 100 μ L of whole blood (seven tubes for seven marker panels, one unstained tube, and eight for compensation control). To lyse red blood cells, 2 mL of freshly-prepared 1 \times NH₄Cl solution was added to each tube and incubated for 10 min at room temperature. Cells were then spun down by centrifuge at 1500 rpm for 6 min at 4 $^{\circ}$ C, washed twice with 2 mL PBS + 2% BSA, and resuspended in 50 μ L of PBS + 2% BSA solution for blocking. Antibodies were added to corresponding tubes and incubated in the dark at 4 $^{\circ}$ C for 45 min. Cells were removed from incubation, washed again twice with PBS + 2% BSA, and resuspended in PBS containing 0.5% formaldehyde. Cell populations were gated on a minimum of 250,000 cells and sorted on basis of 99% purity. Samples were acquired initially on Cyan ADP (Beckman Coulter, Inc.) and later on BD LSRFortessa flow cytometers (Beckton, Dickinson and Company). Logarithmic amplifier linearity and dynamic range were tested with Rainbow beads (Spherotech, Libertyville, IL). Compensation matrix was created using single-color compensation controls to correct for any spectral overlap/spillover. Compensation settings were adjusted using singly-stained peripheral blood samples. Sample analysis was done using FlowJo (Treestar, Inc., Ashland, OR).

2.3. MR imaging

Imaging data were acquired on a single MR scanner, a 3 T MAGNETOM Tim Trio (Siemens, Erlangen, Germany) with maximum gradient slew rate, 200 mT/m/s, maximum gradient strength, 40 mT/m, using a 12 channel receive-only head coil. Sagittal whole brain Magnetization Prepared Rapid Acquisition Gradient Echo images were acquired [parameters: TR/TI/TE: 2300/900/2.91 ms; flip angle: 9 $^{\circ}$; field of view: 256 \times 256 mm; slice thickness: 1 mm; resolution: 1 mm \times 1 mm; slices: 176]. For DTI, a 2D double refocused spin echo sequence with echo planar readout was used for acquisition [parameters: Axial, TR/TE: 9700/90 ms, flip-angle: 90 $^{\circ}$, field of view: 256 \times 256 mm, in-plane resolution: 2 \times 2 mm, slice thickness: 2 mm, slices: 72, bandwidth: 1326 Hz/Px, averages: 1, acceleration factor: 2, directions: 64, b = [0; 1000] s/mm²]. High-resolution MT was acquired using a 3D MT-weighted fast spoiled gradient echo (GRE) pulse sequence with the following parameters: TR = 43 ms, TE = 5 ms, flip angle 10 $^{\circ}$, and 144 1.0-mm slices scanned for axial plane. The scanning matrix was 256 \times 256 with a field of view of 256 mm, resulting in a voxel size of 1.0 \times 1.0 \times 1.0 mm³. To decrease scan time while maintaining resolution, receiver bandwidth was 200 Hz/pixel and an 81.3% rectangular field of view was used.

2.4. Image analysis

For all MR modalities, image quality control was performed visually by a trained operator to ensure that artifacts were not present. Image analysis was blinded to group status (HIV or control). SIENAX (Oxford University, Oxford, England) was used to calculate volumetric measurements for brain parenchyma, ventricular and tissues classes (gray matter, cortical gray matter, white matter, and cerebrospinal fluid), normalized for differences in head size. Smith (2002) SIENAX first extracts a brain and skull image from the subject's structural MPRAGE input image. The skull image is used to determine registration scaling from subject space to standard space (MNI125). This scaling is then used in the affine-registration of the brain image to standard space. This process defines the volumetric scaling factor used to normalize brain volume. To avoid introducing error from blurring associated with registration, tissue segmentation is performed on the original (non-registered) MPRAGE images and volumes are then scaled by the scaling factor to derive the normalized measurements. Freesurfer, Fischl (2002) was used to derive measurements of individual brain regions. To minimize operator variability in manual editing, a semi-automated approach was used. Image quality was assessed based on case by case visual inspection; skull stripping and segmentation results met quality assurance standards for both cortical and subcortical segmentation. To adjust for differences in head size, Freesurfer measurements for individual brain regions were divided by the intracranial cavity volume. DTI parameters, including fractional anisotropy (FA), which is sensitive to white matter integrity, and mean diffusivity (MD), which quantifies water molecular diffusion at levels approximating cellular dimensions, were determined for aggregate 3D volumes of interest. Volumes of interest included regions that have been identified as vulnerable to injury in studies of more advanced infection HIV infection, including cerebral cortex, cerebral white matter, corpus callosum, caudate, putamen, thalamus and hippocampus (Tate, 2011; Anthony and Bell, 2008; Becker, 2011; Chiang, 2007; Cohen, 2010; Thompson, 2012; Thompson, 2006; Wu, 2008; Wu, 2006; Wohlschlaeger, 2009). Parametric FA and MD maps were derived using custom software on a Linux workstation. Eddy-current-induced distortions were corrected in the SE-EPI-DTI images by registering all diffusion-weighted images to the B_0 image for each slice. DTI and MTR parametric maps were coregistered to the anatomical T1 structural image using FLIRT (FMRIB's Linear Registration Tool). For DTI, the B_0 image was used to calculate a transformation matrix between DTI and T1, which was then applied back to the DTI images to align them. For MTR, the mt_0 (no saturation pulse) image was used to calculate a transformation matrix between MTR and T1. Fractional anisotropy (FA) and mean diffusivity (MD) were then calculated using standard equations for all voxels within 3D volumes of interest (Basser and Pierpaoli, 1996b). This approach was also used to calculate MTR for 3D volumes based on $(M_0 - M_S) / M_0$, where M_S and M_0 are the signal intensities with and without the MT saturation pulse.

3. Results

Classification problems were formulated on each HIV subgroup: 0–4 months ($n = 15$), 4–12 months ($n = 15$) and >12–24 months post-infection ($n = 26$) vs. controls ($n = 21$). To determine the discriminative brain measures for the HIV subgroups vs. controls, brain measurements from segmentation, Freesurfer, DTI and MT were used as feature vectors \mathbf{x} , with class label $y = 1$ if the subject was included in the subgroup, $y = -1$ otherwise.

Recursive feature elimination (RFE) based on Support Vector Machines (SVMs) (Guyon et al., 2002; Cao et al., 2014) was implemented. Support Vector Machines (SVMs) learn a weight for each feature in the training process, similar to linear or logistic regression. The difference is that instead of minimizing the square error or the logit loss, SVMs choose the weight vector to maximize the geometric margin

between two classes of samples. Support Vector Machines Recursive Feature Elimination (SVM-RFE) uses the weight magnitude as the ranking criterion. The SVM-RFE algorithm is a well-established and effective wrapper-based feature selection method, which is a backward sequential selection method that removes one feature at a time. SVM-RFE has four general steps: (1) train an SVM on the training set, (2) order features using the weights of the resulting classifier, (3) eliminate features with the smallest weight, and (4) repeat the process with the training set restricted to the remaining features. In this algorithm, the SVM classifier is used to evaluate the discriminative power of the selected subset of features.

$$\min_{\mathbf{w}, b, \xi} \frac{1}{2} \|\mathbf{w}\|_2^2 + c \sum_{i=1}^n \xi_i$$

$$\text{s.t. } y_i \mathbf{w}^T \mathbf{x}_i + b \geq 1 - \xi_i$$

$$\xi_i \geq 0, \forall i = 1, \dots, n,$$

where \mathbf{w} can be regarded as the weight vector of the separating hyperplane in the feature product space, b is the bias, ξ_i is the error of the i th training instance, and c is the trade-off between the margin and empirical loss. It can be solved with use of optimization techniques developed for SVMs, and the weight vector \mathbf{w} can be obtained from

$$\mathbf{w} = \sum_{i=1}^n \alpha_i y_i \mathbf{x}_i$$

where α_i is the dual variable corresponding to each instance.

The objective of SVM-RFE is to find the subset of features that optimizes the performance of the SVM classifier. The algorithm was adapted as recording the sequence of removing features, in order to return a complete ranked list of features. The later a feature is removed, the more discriminating it is. The algorithm is summarized in Fig. 1. A linear kernel based SVM classifier based on the LIBSVM library was adopted in the current framework (Chang and Lin, 2011, 2014).

Table 2 presents classification performance between control and HIV groups at different stages of infection, using the five and ten highest ranked features, as selected by the SVM-RFE algorithm, and using all brain measures without feature selection. Using all brain measures without feature selection fails to optimize classification because the original feature set may contain potentially redundant and irrelevant features. Training a classifier on these features, especially with a limited number of available subjects, as in these data, can result in overfitting

<p>Input:</p> <ul style="list-style-type: none"> - Training examples: $X = [\mathbf{x}_1, \dots, \mathbf{x}_n]$ - Class labels: $\mathbf{y} = [y_1, \dots, y_n]$ - Number of features to be selected: p <p>Initialize:</p> <ul style="list-style-type: none"> - Subset of surviving features: $\mathbf{s} = [1, \dots, m]$ <p>Iterate:</p> <p>Repeat until $length(\mathbf{s}) \leq p$</p> <ul style="list-style-type: none"> - Restrict training examples to good feature indices: $X^* = X(\mathbf{s}, :)$ - Train the classifier: $\mathbf{w} = SVM(X^*, \mathbf{y})$ - Compute the ranking criteria $\mathbf{c} = \mathbf{w}^T \mathbf{w}$ - Find the feature with smallest ranking criterion: $f = argmin(\mathbf{c})$ - Eliminate the feature with smallest ranking criterion: $\mathbf{s} = \mathbf{s}(1: f - 1, f + 1: length(\mathbf{s}))$ <p>Output:</p> <ul style="list-style-type: none"> - Subset of selected features: \mathbf{s}
--

Fig. 1. SVM-RFE algorithm.

Table 2
Classification performance.

Brain measures	Accuracy	Sensitivity (recall)	Specificity	Precision	F1
<i>0–4 months pi</i>					
10 highest ranked	0.917 ± 0.28	0.958 ± 0.14	1.000 ± 0.00	1.000 ± 0.00	0.972 ± 0.09
5 highest ranked	0.833 ± 0.38	0.917 ± 0.19	1.000 ± 0.00	1.000 ± 0.00	0.944 ± 0.13
All	0.722 ± 0.45	0.931 ± 0.18	0.931 ± 0.18	0.931 ± 0.18	0.907 ± 0.15
<i>4–12 months pi</i>					
10 highest ranked	0.889 ± 0.32	0.972 ± 0.12	0.972 ± 0.12	0.972 ± 0.12	0.963 ± 0.11
5 highest ranked	0.667 ± 0.48	0.861 ± 0.23	0.972 ± 0.12	0.972 ± 0.12	0.889 ± 0.16
All	0.583 ± 0.50	0.903 ± 0.20	0.889 ± 0.21	0.889 ± 0.21	0.861 ± 0.17
<i>>12–24 months pi</i>					
10 highest Ranked	0.809 ± 0.40	0.936 ± 0.17	0.968 ± 0.12	0.968 ± 0.12	0.936 ± 0.13
5 highest Ranked	0.596 ± 0.50	0.894 ± 0.21	0.904 ± 0.20	0.904 ± 0.20	0.865 ± 0.17
All	0.426 ± 0.50	0.840 ± 0.24	0.872 ± 0.22	0.872 ± 0.22	0.809 ± 0.17

Averages ± standard deviations of evaluation metrics based on leave one out cross validation. pi: post-infection.

from the perspective of machine learning i.e., poor generality to test data. Therefore, selecting discriminative features is critical to build a robust classifier. On the other hand, classification performance with only the five most discriminating brain measures is not optimal because five features may not be informative enough to learn an effective classifier. Our constructed classifier using the ten highest ranked features, presented in Table 3, achieved the best classification, as shown by various widely used performance metrics (Table 2).

A similar approach was then used to identify features most closely associated with the discriminating brain measures at each stage (Table 3). For this analysis, the most discriminating brain measures were considered as continuous labels and the RFE algorithm was implemented on other features by replacing SVMs with Support Vector Regression Machines (SVRs) (Drucker, et al., 1997). SVRs were trained independently for the top k (default: k = 10) discriminative brain mea-

ures. For each SVR, there is a ranking criterion $c_{(i)} = w_{(i)}^T w_{(i)}$, $i = 1 \dots k$, which were combined via summation, $c = \sum_{i=1}^k c_{(i)}$. The final predictors were determined by removing, in sequence, the feature with the smallest c value in each iteration – the later a feature is removed, the more discriminating the feature. Table 4 presents rankings for the predictors.

4. Conclusions

To inform an understanding of the onset of HIV-induced changes, this study examined the brain at structural, microstructural (Diffusion Tensor) and macromolecular (Magnetization Transfer) levels in individuals infected less than 4 months (antibody nonreactive, Primary HIV), 4–12 months post-infection (pi) and in early chronic infection, defined

Table 3
Most discriminative brain measurements by stage (highest rank: top).

Brain measurement	HIV mean ± SD	Control mean ± SD
<i>0–4 months post-infection</i>		
Cortical gray matter volume	6.7244e+05 ± 6.8826e+04	7.1210e+05 ± 3.4820e+04
DTI FA: mid-posterior CC	5.9215e-01 ± 7.8661e-02	6.3608e-01 ± 3.8864e-02
3rd ventricle volume	6.4700e-04 ± 1.2523e-04	5.5920e-04 ± 1.1147e-04
Lateral ventricle volume	6.7434e-03 ± 2.6941e-03	8.6943e-03 ± 3.7096e-03
Brainstem volume	1.4313e-02 ± 8.3209e-04	1.3477e-02 ± 9.6935e-04
DTI FA: anterior CC	6.4761e-01 ± 5.2708e-02	6.9982e-01 ± 5.5296e-02
DTI MD: aggregate white matter	7.2813e-04 ± 2.1672e-05	7.3381e-04 ± 1.3945e-05
Cerebral cortex volume	3.1773e-01 ± 3.4012e-02	3.3188e-01 ± 1.8838e-02
DTI FA: corpus callosum	6.6370e-01 ± 3.9193e-02	6.9255e-01 ± 2.2936e-02
Gray matter volume	8.8307e+05 ± 7.7013e+04	9.2598e+05 ± 5.4841e+04
<i>4–12 months post-infection</i>		
DTI FA: corpus callosum	6.6062e-01 ± 4.3113e-02	6.9255e-01 ± 2.2936e-02
DTI FA: cerebral white matter	4.4810e-01 ± 1.4325e-02	4.6036e-01 ± 1.4384e-02
Caudate volume	5.1246e-03 ± 6.7222e-04	4.7463e-03 ± 4.7151e-04
4th ventricle volume	1.0509e-03 ± 2.4087e-04	1.3410e-03 ± 4.2966e-04
DTI FA: anterior CC	6.5497e-01 ± 3.0413e-02	6.9982e-01 ± 5.5296e-02
DTI FA: hippocampus	1.7001e-01 ± 8.8006e-03	1.6015e-01 ± 1.3612e-02
White matter volume	6.9372e+05 ± 2.2541e+04	6.8139e+05 ± 4.1380e+04
MTR: hippocampus	3.5146e+01 ± 1.1827e+00	3.4391e+01 ± 2.3965e+00
Posterior CC volume	5.8357e-04 ± 1.3621e-04	6.1219e-04 ± 7.4019e-05
Amygdala volume	2.4801e-03 ± 3.1429e-04	2.3440e-03 ± 1.4224e-04
<i>Over 12–24 months post-infection</i>		
Cerebral cortex volume	3.1552e-01 ± 2.3740e-02	3.3188e-01 ± 1.8838e-02
DTI FA: corpus callosum	6.6903e-01 ± 4.4107e-02	6.9255e-01 ± 2.2936e-02
DTI FA: hippocampus	1.6806e-01 ± 2.0701e-02	1.6015e-01 ± 1.3612e-02
Cortical gray matter volume	6.8367e+05 ± 4.4681e+04	7.1210e+05 ± 3.4820e+04
DTI MD: hippocampus	9.3385e-04 ± 3.5553e-05	9.4498e-04 ± 3.6070e-05
MTR: central CC	4.3771e+01 ± 2.6509e+00	4.4982e+01 ± 2.4494e+00
DTI FA: whole brain	2.8722e-01 ± 1.0762e-02	2.8599e-01 ± 9.9421e-03
Caudate volume	4.8686e-03 ± 4.5856e-04	4.7463e-03 ± 4.7151e-04
Inferior lateral ventricle vol.	3.3846e-04 ± 1.5106e-04	2.7575e-04 ± 1.2414e-04
DTI MD: anterior CC	9.0638e-04 ± 1.2362e-04	8.9962e-04 ± 1.1957e-04

Table 4
Ranked determinants of brain alterations (highest: top).

0–4 months post-infection
CBC: CD4+/CD8+
Flow: CD8+ T cells
Luminex: TNF α
CSF: GM-CSF
CBC: absolute basophils
Luminex: IL-6
Flow: %CD36+, T cells
Flow: %CD45RO+, CD16+ monocytes
CBC: hematocrit
Luminex: MMP-7
Luminex: fractalkine
Luminex: MMP-1
Flow: %CD3–CD56+CD16–, NK cells
Flow: %CD36+, CD33+ monocytes
CBC: absolute CD4+
Luminex: MCP-1
4–12 months post-infection
CBC: %CD3+, total lymphocytes
Flow: %B cells, total lymphocytes
Flow: %CD36+, CD33+ monocytes
Luminex: MMP-1
Alcohol use frequency, past month
Flow: %CD4+,CD3+CD56+CD16– NKT cells
Flow: % singlets, lymphocytes
Flow: %T Cells, total lymphocytes
Flow: %CD56+, CD16– monocytes
CBC: monocytes percent
Luminex: IL-9
Length of infection
Substance use: marijuana, past 6 months
Flow: %CD45RO+, CD16+ monocytes
Over 12–24 months post-infection
Age
Flow: %CD3–CD56+CD16+, NK cells
Flow: %CD36+, CD33+ monocytes
Luminex: MMP-1
Flow: %CD4+,CD3+CD56–CD16+ NKT cells
Luminex: TNF α
CBC: eosinophils percent
Emtricitabine exposure (an NRTI)
Luminex: MDC
Luminex: MMP-10
Luminex: IL-4
Flow: %CD4–CD8–,CD3–CD56+CD16– NK cells
Flow: %CD71+, CD33+ monocytes
Luminex: MIP-1 β

here as approximately 12–24 months pi. Discriminating brain features in Primary Infection involved gray matter, white matter and ventricular measurements (Table 3). Cortical Gray Matter Volume was highest ranked, with reduced levels compared to controls (Fig. 2). Examination of the means for other highly ranked features presented in Table 3 suggests a similar pattern for volumetric measurements of cerebral cortex and gray matter with enlargement of brainstem, third and lateral ventricles. Findings for microstructural measurements (DTI) are consistent with diffusion restriction in white matter. Three of the most highly ranked features in Primary Infection involved anisotropy measurements of corpus callosum (Fig. 2).

Alterations quantified in Primary Infection likely reflect acute neuroinflammation following initial viral invasion of the brain. The blood brain barrier generally shelters neural tissue from potential toxins, however, permeability may be altered in immune perturbances of the initial viral host interaction (McMichael, 2010; Borrow and Bhardwaj, 2008; Stacey, 2009). Consistent with very early brain involvement, virus can be detected in the cerebrospinal fluid in Acute HIV and the initial symptom presentation includes headache (Valcour, 2012b). Abnormalities in gray matter and ventricular expansion are apparent on clinical MR in patients with Acute HIV meningoencephalitis (Yoshizawa et al., 2007).

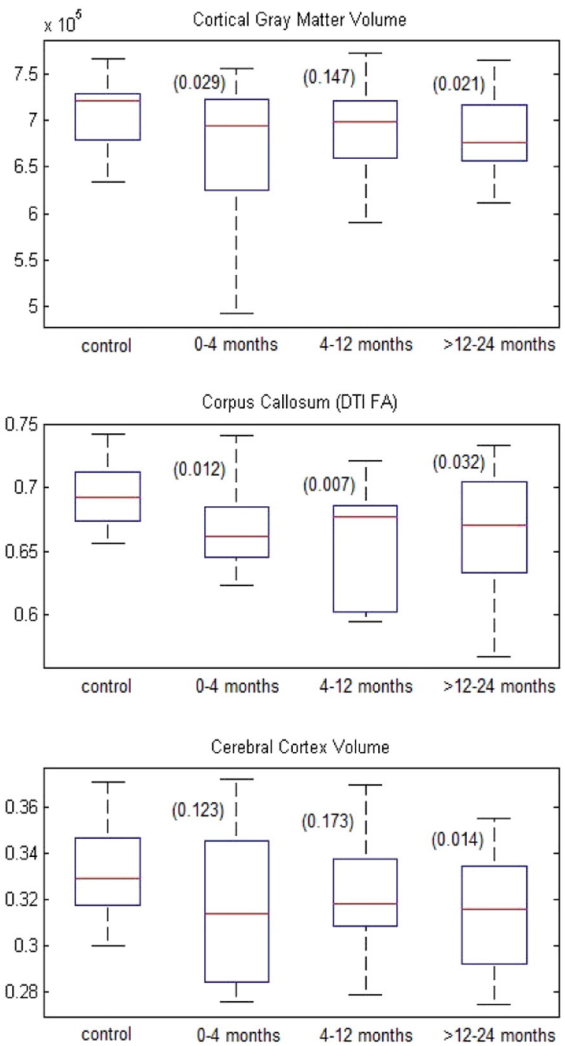


Fig. 2. Group differences of most discriminating brain measures. Group differences for highest ranked brain measures at each stage: 0–4 months (cortical gray matter volume), 4–12 months (corpus callosum DTI FA) and >12–24 months (cerebral cortex volume) post-infection. HIV groups were compared with controls using t-tests. FA (fractional anisotropy).

An autopsy only 15 days following an iatrogenic infection revealed neuropathological findings in meninges, cortex and subcortical regions (Davis, 1992).

The brain was also examined in the period immediately following the adaptive immune response (4–12 months pi). This is an immunologically significant period in which viral and immune activation set points become established (Mellors, 1996; Deeks, 2004). Evidence that ART within the first year confers greater benefit (e.g. Le, 2013; Burdo, 2011) motivated investigation of the immediately subsequent period: >12–24 months pi. Highly ranked features at 4–12 months reveal a prominent pattern of subcortical findings and involvement of cerebral white matter (Table 3). Anisotropy measurements of corpus callosum were highest ranked in this period (Table 3; Fig. 2). Other callosal and white matter measures were also highly ranked. Examination of the means in Table 3 suggests findings consistent with swelling in this period immediately following seroconversion, in aggregate brain white matter, caudate and amygdala. Hippocampal involvement, which has been reported at autopsy (Anthony and Bell, 2008) was quantified with two separate modalities (FA and MTR). The pattern observed >12–24 months pi was consistent with both prior periods (Table 3). Cortical and cortical gray matter volume were reduced with microstructural anisotropy alterations in corpus callosum (Fig. 2).

Examination of group means suggests ventricular expansion (inferior lateral) and ongoing involvement of caudate, hippocampus and individual callosal segments.

The dramatic immune perturbances characteristic of the initial virus host interaction are generally followed by a prolonged asymptomatic period in association with host defense (McMichael, 2010; Schacker, 1996). In the brain, however, earliest alterations do not appear to resolve with seroconversion. Alterations in corpus callosum and in the anterior callosal segment were identified in all studied periods. Alterations in caudate, considered a predilection site of viral injury and in hippocampus were quantified in the period immediately following seroconversion (4–12 months) and persisted thereafter. Brain alterations evident over 12 months pi were consistent with ongoing neuroinflammation, loss of white matter integrity and atrophy.

This analysis also used data mining to identify the factors associated with brain alterations observed in each period. This analysis considered subject characteristics, medical history, clinical laboratory measures, lymphocyte and other immune cell subsets, cytokines, chemokines and behavioral measures (e.g. alcohol/substance use). The factors most closely associated with the earliest alterations in the brain included critical markers of immunologic status – plasma CD4+/CD8+ ratio and CD8+ T cells (Table 4). Other factors associated with brain alterations in primary infection (0–4 months pi) included: TNF α , basophils, IL-6, hematocrit, CD36+ T Cells, CD16+CD45RO+ monocytes, MMPs (–7 and –1), fractalkine, CD3–CD56+CD16– NK cells, CD33+CD36+ monocytes, MCP-1, as well as CD4+ T cells. GM-CSF, which stimulates monocyte/granulocyte expansion, was highest ranked in CSF. The finding for basophils (mast cell precursors) suggests potential mast cell mediated meningeal inflammation (Ransohoff and Brown, 2012). Factors most highly associated with brain alterations at 4–12 months pi included plasma MMP-1, IL-9, populations of circulating monocytes, as well as infection duration, alcohol and marijuana use. Age, which has been established as a risk factor for HIV neurocognitive impairment (e.g. Valcour, 2004), was highest ranked in those infected more than 12 months. Age ranked higher than all other factors identified in this period, which included plasma MMP-1, TNF α , eosinophils, emtricitabine exposure, CD33+CD36+ monocytes, total CD3–CD56+CD16+ NK cells, MDC, MMP-10, IL-4, CD3–CD56+CD16– (%CD4–CD8–) NK cells, CD33+CD71+ monocytes, and MIP-1 β .

These findings clarify evidence implicating a legacy event involving severe immunosuppression in cognitive deterioration (Valcour, 2006; Ellis et al., 2010, 2011). Onset of neural injury may date to massive CD4+ loss and severe immunosuppression that occurs in Primary infection. Viremia reaches staggering peak levels within only 21–28 days pi (Gasper-Smith, 2008). Uncontrolled viremia in the initial virus host interaction is accompanied by massive loss of CD4+ T cells and a cytokine storm. HIV subverts immune control/host defense by infecting cells critical to pathogen response – CD4+ T cells and monocyte/macrophages, which serve as a vehicle for brain ingress, facilitated by immune activation, MMPs and cytokines/chemokines, such as TNF α , IL-6 (similarly, hematocrit), fractalkine and MCP-1 (Gartner and Liu, 2002; MacLean, 2004). Infected macrophages in the meninges (Lamers, 2011), subarachnoid space and parenchyma induce inflammatory cascades (Lindl, 2010) involving cytokines, chemokines and other immune mediators which disturb neuronal and glial function (Kaul and Lipton, 2006). Neurons may be injured from exposure to viral proteins, as well as immune-stimulated macrophages/microglia (Kaul, 2009). The brain has a limited repertoire for responding to insult and injury. Microglia and astrocytes, which do not have direct counterparts in the periphery, are the primary mediators of these responses in the brain (Ransohoff and Brown, 2012). The viral protein, tat, for example, increases intracellular calcium, potentiates excitotoxicity, and induces apoptosis (Eugenin, 2007; Haughey, 2001). Transient exposure to viral proteins may cause progressive neuropathological changes for days (Nath, 1999).

Of markers in plasma, MMP-1 was highly ranked in all periods studied. MMPs are potent proteolytic enzymes that when dysregulated pose serious risk of tissue destruction (Sternlicht and Werb, 2001). MMPs have been implicated in HIV associated brain injury (Suryadevara, 2003; Dhar, 2006). MMP-1 may modulate the neurotoxicity of HIV viral proteins (Conant, 2004; Rumbaugh, 2006). Additionally, prolonged astrocyte activation may result in elevated MMP-1 levels (Suryadevara, 2003). Circulating MMP-1 levels correlate with the severity of brain injury in advanced infection (e.g. Ragin, 2009). CD33+CD36+ monocytes, which were also identified in all three periods, have been implicated in impaired ingestion of damaged cells and pathogen, dysregulated lipid metabolism, atherosclerosis, and cardiovascular disease (Olivetta, 2014; Feeney, 2013). CD16+CD45RO+ monocytes, a subset of activated monocytes, were highly ranked specifically within the first year of infection, consistent with findings from brain autopsy (Cosenza-Nashat, 2006). The first year of infection may also be time-critical for optimizing preservation of immune function (Le, 2013) and potentially for preserving the brain. Treatment status was not identified as a highly ranked feature of the most discriminating brain alterations, other than the finding for Emtricitabine exposure, which was identified >12–24 months pi. This study, however, is based on an observational cohort in which timing and duration of antiretroviral therapy varied in individual participants and the percentage of naïve and ART participants differed in the HIV subgroups. Findings of early brain involvement underscore the importance of further studies clarifying whether ART in initial infection confers neuroprotective benefit.

When interpreting these findings, it is important to appreciate that microstructural (DTI) and macromolecular (MTR) parameters were only measured in select regions – early brain involvement may extend to regions not interrogated here. Additionally, brain alterations observed in early infection may also reflect neuroreparative efforts (e.g. neurogenesis, hippocampus) changes (Kaul, 2009). Alterations in only a single period (e.g. brainstem, amygdala) may reflect short-lived or evolving changes (e.g. localized neuroinflammation), transient changes in surrounding brain regions, or pseudonormalization. If heterogeneous changes are occurring within a given structure (e.g. swelling and atrophic changes), this may yield “pseudonormal” measures that underestimate early brain involvement. Nevertheless, the consistent pattern observed in three different samples across three different time periods support the premise of onset of brain alterations in early HIV infection. Moreover, other studies have found brain changes early in HIV infection (Valcour, 2012b; Peluso, 2013; Spudich, 2011; Ances, 2009; Wang, 2011) reporting similar findings, such as altered neuronal integrity in frontal cortex with microglial activation in basal ganglia and an association with circulating monocytes across the first year of infection (e.g. Lentz, 2011).

These findings shed light on brain changes induced by HIV and their evolution in initial stages of infection. The severity of immunosuppression in the initial virus host interaction, possibly mediated by host factors associated with immune compromise (e.g. alcohol, substance use, age), may determine the relative degree of early brain involvement. While transient, uncontrolled viremia and immunosuppression in Primary Infection may have lasting effects on the brain. The brain alterations detected in early infection mirror the atrophy, striatal and callosal injury, seen in advanced HIV infection (e.g. Becker, 2011; Thompson, 2006; Thompson, 2005) and at autopsy (Wohlschlaeger, 2009). Early changes, for example, in the cerebral cortex, may also be broadly relevant to the abnormalities that have been identified at various levels in advanced HIV infection, such as patterns of gray matter loss and aberrant function in localized cortical areas shown by magnetoencephalography (Becker, 2012a,b, 2013; Wilson, 2013a,b, 2015), as well as alterations in brain resting state functional connectivity shown by fMRI (Thomas, 2013).

Similarly, many of the factors associated with the earliest brain alterations, such as markers of immune activation and of circulating

monocytes, also predict neurological outcome in advanced infection (Ragin, 2009; Seigniny, 2004, 2007; Ragin, 2010, 2011; Gartner, 2000). This analysis identified abnormalities in caudate and hippocampus within only 4–12 months pi. Early onset of neural injury may explain why atrophy e.g. in basal ganglia, corresponds with duration of infection, despite successful viral suppression by ART (Becker, 2011). Early onset of neural injury may explain why treatment may fail to confer neuroprotection (Brew, 2007). Evidence of ongoing brain alterations across the period in which systemic viral suppression occurs supports the premise that a viral reservoir is established in the brain very early in infection, that may preclude viral eradication in the host. Treatment in acute infection may confer greater neuroprotective benefit by suppressing the intensity of initial viremia, thereby preserving CD4+ T cells and immune function while potentially limiting early seeding of the brain and other reservoirs. Alterations involving the corpus callosum and in the anterior callosal segment were identified in all periods, suggesting that measures in this region may represent promising biomarkers of early brain involvement in HIV infection with potential utility for quantifying effects of intervention.

Acknowledgments

This work was supported by the National Institute of Mental Health (R01-MH080636). The authors appreciate the services of the Center for Translational Imaging. All authors state they have no conflict of interests related to this manuscript.

References

- Ances, B.M., et al., 2009. Resting cerebral blood flow: a potential biomarker of the effects of HIV in the brain. *Neurology* 73 (9), 702–708. <http://dx.doi.org/10.1212/WNL.0b013e3181b59a9719720977>.
- Anthony, I.C., Bell, J.E., 2008. The neuropathology of HIV/AIDS. *Int. Rev. Psychiatry* 20 (1), 15–24. <http://dx.doi.org/10.1080/0954026070186203718240059>.
- Basser, P.J., Pierpaoli, C., 1996a. Microstructural and physiological features of tissues elucidated by quantitative-diffusion-tensor MRI. *J. Magn. Reson. B* 111 (3), 209–219. <http://dx.doi.org/10.1006/jmrb.1996.00868661285>.
- Basser, P.J., Pierpaoli, C., 1996b. Microstructural and physiological features of tissues elucidated by quantitative-diffusion-tensor MRI. *J. Magn. Reson. B* 111 (3), 209–219. <http://dx.doi.org/10.1006/jmrb.1996.00868661285>.
- Becker, J.T., et al., 2011. Subcortical brain atrophy persists even in HAART-regulated HIV disease. *Brain Imaging Behav.* 5 (2), 77–85. <http://dx.doi.org/10.1007/s11682-011-9113-821264551>.
- Becker, J.T., et al., 2012a. Potential utility of resting-state magnetoencephalography as a biomarker of CNS abnormality in HIV disease. *J. Neurosci. Methods* 206 (2), 176–182. <http://dx.doi.org/10.1016/j.jneumeth.2012.02.02222414786>.
- Becker, J.T., et al., 2012b. Functional connectivity measured with magnetoencephalography identifies persons with HIV disease. *Brain Imaging Behav.* 6 (3), 366–373. <http://dx.doi.org/10.1007/s11682-012-9149-422328062>.
- Becker, K.M., et al., 2011. Decreased MEG beta oscillations in HIV-infected older adults during the resting state. *J. Neurovirol.* 19 (6), 586–594. <http://dx.doi.org/10.1007/s13365-013-0220-824297500>.
- Borrow, P., Bhardwaj, N., 2008. Innate immune responses in primary HIV-1 infection. *Curr. Opin. H.I.V. A.I.D.S.* 3 (1), 36–44. <http://dx.doi.org/10.1097/COH.0b013e3282f2bce719372942>.
- Brew, B.J., 2007. Lost in translation: again, another failed neuroprotection trial. *Neurol.* 69 (13), 1308–1309. <http://dx.doi.org/10.1212/01.wnl.0000277530.05450.ff17893290>.
- Burdo, T.H., et al., 2011. Soluble CD163 made by monocyte/macrophages is a novel marker of HIV activity in early and chronic infection prior to and after anti-retroviral therapy. *J. Infect. Dis.* 204 (1), 154–163. <http://dx.doi.org/10.1093/infdis/jir21421628670>.
- Cao, B., et al., 2014. Tensor-based multi-view feature selection with applications to brain diseases. *IEEE International Conference on Data Mining, Shenzhen, China*.
- Chang, C.-C., Lin, C.-J., 2011. LIBSVM: a library for support vector machines. *ACM. Transactions Intell. Syst. Technol.* 2 (3), 1–27. <http://dx.doi.org/10.1145/1961189.1961199>.
- Chang, C.-C., Lin, C.-J., 2014. LIBSVM: A Library for Support Vector Machines. [Software] [cited 2015 January 1] available from: <http://www.csie.ntu.edu.tw/~cjlin/libsvm/>.
- Chiang, M.C., et al., 2007. 3D pattern of brain atrophy in HIV/AIDS visualized using tensor-based morphometry. *Neuroimage* 34 (1), 44–60. <http://dx.doi.org/10.1016/j.neuroimage.2006.08.03017035049>.
- Cohen, R.A., et al., 2010. Effects of nadir CD4 count and duration of human immunodeficiency virus infection on brain volumes in the highly active antiretroviral therapy era. *J. Neurovirol.* 16 (1), 25–32. <http://dx.doi.org/10.3109/135502809035524200113183>.
- Conant, K., et al., 2004. Matrix metalloproteinase 1 interacts with neuronal integrins and stimulates dephosphorylation of Akt. *J. Biol. Chem.* 279 (9), 8056–8062. <http://dx.doi.org/10.1074/jbc.M30705120014679206>.
- Cosenza-Nashat, M.A., et al., 2006. CD45 isoform expression in microglia and inflammatory cells in HIV-1 encephalitis. *Brain Pathol.* 16 (4), 256–265. <http://dx.doi.org/10.1111/j.1750-3639.2006.00027.x17107594>.
- Davis, L.E., et al., 1992. Early viral brain invasion in iatrogenic human immunodeficiency virus infection. *Neurol.* 42 (9), 1736–1739. <http://dx.doi.org/10.1212/WNL.42.9.17361513462>.
- Deeks, S.G., et al., 2004. Immune activation set point during early HIV infection predicts subsequent CD4+ T-cell changes independent of viral load. *Blood* 104 (4), 942–947. <http://dx.doi.org/10.1182/blood-2003-09-333315117761>.
- Dhar, A., et al., 2006. Novel role of TGF-beta in differential astrocyte-TIMP-1 regulation: implications for HIV-1-dementia and neuroinflammation. *J. Neurosci. Res.* 83 (7), 1271–1280. <http://dx.doi.org/10.1002/jnr.2078716496359>.
- Drucker, H., et al., 1997. Support vector regression machines. *Advances in Neural Information Processing Systems* 9, 155–161.
- Ellis, R., Heaton, R., Letendre, S., Badiee, J., Munoz-Moreno, J., Vaida, F., Clifford, D., Gelman, B., Simpson, D., Grant, I., Charter Group, 2010. Higher CD4 nadir is associated with reduced rates of HIV-associated neurocognitive disorders in the CHARTER study: potential implications for early treatment initiation. *Conference on Retroviruses and Opportunistic Infections, San Francisco, CA*.
- Ellis, R.J., et al., 2011. CD4 nadir is a predictor of HIV neurocognitive impairment in the era of combination antiretroviral therapy. *A.I.D.S.* 25 (14), 1747–1751. <http://dx.doi.org/10.1097/QAD.0b013e32834a40cd21750419>.
- Eugenin, E.A., et al., 2007. HIV-tat induces formation of an LRP-PSD-95- NMDAR-nNOS complex that promotes apoptosis in neurons and astrocytes. *Proc. Natl. Acad. Sci. U. S. A.* 104 (9), 3438–3443. <http://dx.doi.org/10.1073/pnas.061169910417360663>.
- Feeney, E.R., et al., 2013. The expression of cholesterol metabolism genes in monocytes from HIV-infected subjects suggests intracellular cholesterol accumulation. *J. Infect. Dis.* 207 (4), 628–637. <http://dx.doi.org/10.1093/infdis/jis72323204179>.
- Fischl, B., et al., 2002. Whole brain segmentation: automated labeling of neuroanatomical structures in the human brain. *Neuron* 33 (3), 341–355. [http://dx.doi.org/10.1016/S0896-6273\(02\)00569-X11832223](http://dx.doi.org/10.1016/S0896-6273(02)00569-X11832223).
- Gartner, S., 2000. HIV infection and dementia. *Science* 287 (5453), 602–604. <http://dx.doi.org/10.1126/science.1111111>.
- Gartner, S., Liu, Y., 2002. Insights into the role of immune activation in HIV neuropathogenesis. *J. Neurovirol.* 8 (2), 69–75. <http://dx.doi.org/10.1080/1355028029004952511935459>.
- Gasper-Smith, N., et al., 2008. Induction of plasma (TRAIL), TNFR-2, Fas ligand, and plasma microparticles after human immunodeficiency virus type 1 (HIV-1) transmission: implications for HIV-1 vaccine design. *J. Virol.* 82 (15), 7700–7710. <http://dx.doi.org/10.1128/JVI.00605-0818508902>.
- Guyon, I., et al., 2002. Gene selection for cancer classification using support vector machines. *Mach. Learn.* 46 (1–3), 389–422.
- Haughey, N.J., et al., 2001. HIV-1 Tat through phosphorylation of NMDA receptors potentiates glutamate excitotoxicity. *J. Neurochem.* 78 (3), 457–467. <http://dx.doi.org/10.1046/j.1471-4159.2001.00396.x11483648>.
- Kaul, M., 2009. HIV-1 associated dementia: update on pathological mechanisms and therapeutic approaches. *Curr. Opin. Neurol.* 22 (3), 315–320. <http://dx.doi.org/10.1097/WCO.0b013e3283293f3c19300249>.
- Kaul, M., Lipton, S.A., 2006. Mechanisms of neuroimmunity and neurodegeneration associated with HIV-1 infection and AIDS. *J. Neuroimmune Pharmacol.* 1 (2), 138–151. <http://dx.doi.org/10.1007/s11481-006-9011-918040780>.
- Keating, S.M., et al., 2012. Lower-sensitivity and avidity modifications of the VITROS anti-HIV 1 + 2 assay for detection of recent HIV infections and incidence estimation. *J. Clin. Microbiol.* 50 (12), 3968–3976. <http://dx.doi.org/10.1128/JCM.01454-1223035182>.
- Lamers, S.L., et al., 2011. HIV-1 phylogenetic analysis shows HIV-1 transits through the meninges to brain and peripheral tissues. *Infect. Genet. Evol.* 11 (1), 31–37. <http://dx.doi.org/10.1016/j.meegid.2010.10.01621055482>.
- Le, T., et al., 2013. Enhanced CD4+ T-cell recovery with earlier HIV-1 antiretroviral therapy. *N. Engl. J. Med.* 368 (3), 218–230. <http://dx.doi.org/10.1056/NEJMoa111018723323898>.
- Lentz, M.R., et al., 2011. Alterations in brain metabolism during the first year of HIV infection. *J. Neurovirol.* 17 (3), 220–229. <http://dx.doi.org/10.1007/s13365-011-0030-921494901>.
- Lindl, K.A., et al., 2010. HIV-associated neurocognitive disorder: pathogenesis and therapeutic opportunities. *J. Neuroimmune Pharmacol.* 5 (3), 294–309. <http://dx.doi.org/10.1007/s11481-010-9205-z20396973>.
- MacLean, A.G., et al., 2004. Activation of the blood–brain barrier by SIV (simian immunodeficiency virus) requires cell-associated virus and is not restricted to endothelial cell activation. *Biochem. Soc. Trans.* 32 (5), 750–752. <http://dx.doi.org/10.1042/BST0320750>.
- McMichael, A.J., et al., 2010. The immune response during acute HIV-1 infection: clues for vaccine development. *Nat. Rev. Immunol.* 10 (1), 11–23. <http://dx.doi.org/10.1038/nri267420010788>.
- Mellors, J.W., et al., 1996. Prognosis in HIV-1 infection predicted by the quantity of virus in plasma. [erratum in: *science* 1997 January 3; 275(5296):14]. *Science* 272 (5265), 1167–1170. <http://dx.doi.org/10.1126/science.272.5265.11678638160>.
- Nath, A., et al., 1999. Transient exposure to HIV-1 Tat protein results in cytokine production in macrophages and astrocytes: a hit and run phenomenon. *J. Biol. Chem.* 274 (24), 17098–17102. <http://dx.doi.org/10.1074/jbc.274.24.1709810358063>.
- Olivetta, E., et al., 2014. HIV-1 Nef impairs key functional activities in human macrophages through CD36 downregulation. *PLOS One* 9 (4), e93699. <http://dx.doi.org/10.1371/journal.pone.009369924705461>.
- Peluso, M.J., et al., 2013. Cerebrospinal fluid and neuroimaging biomarker abnormalities suggest early neurological injury in a subset of individuals during primary HIV infection. *J. Infect. Dis.* 207 (11), 1703–1712. <http://dx.doi.org/10.1093/infdis/jit08823460748>.

- Ragin, A.B., et al., 2009. Serum matrix metalloproteinase levels correlate with brain injury in human immunodeficiency virus infection. *J. Neurovirol.* 15 (3), 275–281. <http://dx.doi.org/10.1080/1355028090291327119444696>.
- Ragin, A.B., et al., 2010. Biomarkers of neurological status in HIV infection: a 3-year study. *Proteomics Clin. Appl.* 4 (3), 295–303. <http://dx.doi.org/10.1002/prca.20090008321137050>.
- Ragin, A.B., et al., 2011. Marked relationship between matrix metalloproteinase 7 and brain atrophy in HIV infection. *J. Neurovirol.* 17 (2), 153–158. <http://dx.doi.org/10.1007/s13365-011-0018-521302026>.
- Ransohoff, R.M., Brown, M.A., 2012. Innate immunity in the central nervous system. *J. Clin. Invest.* 122 (4), 1164–1171. <http://dx.doi.org/10.1172/JCI5864422466658>.
- Rumbaugh, J., et al., 2006. Interaction of HIV Tat and matrix metalloproteinase in HIV neuropathogenesis: a new host defense mechanism. *F.A.S.E.B. J.* 20 (10), 1736–1738. <http://dx.doi.org/10.1096/fj.05-5619fje16807369>.
- Schacker, T., et al., 1996. Clinical and epidemiologic features of primary HIV infection. [see comment] [erratum appears in *Ann Intern Med* 1997 January 15; 126(2):174]. *Ann. Intern. Med.* 125 (4), 257–264. <http://dx.doi.org/10.7326/0003-4819-125-4-199608150-000018678387>.
- Sevigny, J.J., et al., 2004. Evaluation of HIV RNA and markers of immune activation as predictors of HIV-associated dementia. *Neurol.* 63 (11), 2084–2090. <http://dx.doi.org/10.1212/01.WNL.0000145763.68284.1515596754>.
- Sevigny, J.J., et al., 2007. An evaluation of neurocognitive status and markers of immune activation as predictors of time to death in advanced HIV infection. *Arch. Neurol.* 64 (1), 97–102. <http://dx.doi.org/10.1001/archneur.64.1.9717210815>.
- Smith, S.M., et al., 2002. Accurate, robust, and automated longitudinal and cross-sectional brain change analysis. *Neuroimage* 17 (1), 479–489. <http://dx.doi.org/10.1006/nimg.2002.104012482100>.
- Spudis, S., et al., 2011. Central nervous system immune activation characterizes primary human immunodeficiency virus 1 infection even in participants with minimal cerebrospinal fluid viral burden. *J. Infect. Dis.* 204 (5), 753–760. <http://dx.doi.org/10.1093/infdis/jir38721844301>.
- Stacey, A.R., et al., 2009. Induction of a striking systemic cytokine cascade prior to peak viremia in acute human immunodeficiency virus type 1 infection, in contrast to more modest and delayed responses in acute hepatitis B and C virus infections. *J. Virol.* 83 (8), 3719–3733. <http://dx.doi.org/10.1128/JVI.01844-0819176632>.
- Sternlicht, M.D., Werb, Z., 2001. How matrix metalloproteinases regulate cell behavior. *Annu. Rev. Cell Dev. Biol.* 17, 463–516. <http://dx.doi.org/10.1146/annurev.cellbio.17.1.46311687497>.
- Suryadevara, R., et al., 2003. Regulation of tissue inhibitor of metalloproteinase-1 by astrocytes: links to HIV-1 dementia. *Glia* 44 (1), 47–56. <http://dx.doi.org/10.1002/glia.1026612951656>.
- Tate, D.F., et al., 2011. Regional areas and widths of the midsagittal corpus callosum among HIV-infected patients on stable antiretroviral therapies. *J. Neurovirol.* 17 (4), 368–379. <http://dx.doi.org/10.1007/s13365-011-0033-621556960>.
- Thomas, J.B., et al., 2013. Pathways to neurodegeneration: effects of HIV and aging on resting-state functional connectivity. *Neurology* 80 (13), 1186–1193. <http://dx.doi.org/10.1212/WNL.0b013e318288792b23446675>.
- Thompson, M.A., et al., 2012. Antiretroviral treatment of adult HIV infection: 2012 recommendations of the International Antiviral Society-USA panel. *JAMA* 308 (4), 387–402. <http://dx.doi.org/10.1001/jama.2012.796122820792>.
- Thompson, P.M., et al., 2005. Thinning of the cerebral cortex visualized in HIV/AIDS reflects CD4+ T lymphocyte decline. *Proc. Natl. Acad. Sci. U. S. A.* 102 (43), 15647–15652. <http://dx.doi.org/10.1073/pnas.050254810216227428>.
- Thompson, P.M., et al., 2006. 3D mapping of ventricular and corpus callosum abnormalities in HIV/AIDS. *Neuroimage* 31 (1), 12–23. <http://dx.doi.org/10.1016/j.neuroimage.2005.11.04316427319>.
- Valcour, V., et al., 2004. Age, apolipoprotein E4, and the risk of HIV dementia: the Hawaii aging with HIV cohort. *J. Neuroimmunol.* 157 (1–2), 197–202. <http://dx.doi.org/10.1016/j.jneuroim.2004.08.02915579298>.
- Valcour, V., et al., 2006. Lowest ever CD4 lymphocyte count (CD4 nadir) as a predictor of current cognitive and neurological status in human immunodeficiency virus type 1 infection – the Hawaii aging with HIV cohort. *J. Neurovirol.* 12 (5), 387–391. <http://dx.doi.org/10.1080/1355028060091533917065131>.
- Valcour, V., et al., 2012a. Central nervous system viral invasion and inflammation during acute HIV infection. *J. Infect. Dis.* 206 (2), 275–282. <http://dx.doi.org/10.1093/infdis/jis32622551810>.
- Valcour, V., et al., 2012b. Central nervous system viral invasion and inflammation during acute HIV infection. *J. Infect. Dis.* 206 (2), 275–282. <http://dx.doi.org/10.1093/infdis/jis32622551810>.
- Wang, X., et al., 2011. Abnormalities in resting-state functional connectivity in early human immunodeficiency virus infection. *Brain Connect.* 1 (3), 207–217. <http://dx.doi.org/10.1089/brain.2011.001622433049>.
- Wilson, T.W., et al., 2013a. Abnormal MEG oscillatory activity during visual processing in the prefrontal cortices and frontal eye-fields of the aging HIV brain. *PLOS One* 8 (6), e66241. <http://dx.doi.org/10.1371/journal.pone.0066241> [PubMed: 23840428].
- Wilson, T.W., et al., 2013b. Functional brain abnormalities during finger-tapping in HIV-infected older adults: a magnetoencephalography study. *J. Neuroimmune Pharmacol.* 8 (4), 965–974. <http://dx.doi.org/10.1007/s11481-013-9477-123749418>.
- Wilson, T.W., et al., 2015. Multimodal neuroimaging evidence of alterations in cortical structure and function in HIV-infected older adults. *Hum. Brain Mapp.* 36 (3), 897–910. <http://dx.doi.org/10.1002/hbm.2267425376125>.
- Wohlschlaeger, J., et al., 2009. White matter changes in HIV-1 infected brains: A combined gross anatomical and ultrastructural morphometric investigation of the corpus callosum. *Clin. Neurol. Neurosurg.* 111 (5), 422–429. <http://dx.doi.org/10.1016/j.clineuro.2008.12.00619185416>.
- Wolff, S.D., Balaban, R.S., 1994. Magnetization transfer imaging: practical aspects and clinical applications. *Radiology* 192 (3), 593–599. <http://dx.doi.org/10.1148/radiology.192.3.80589198058919>.
- Wu, Y., et al., 2006. Diffusion alterations in corpus callosum of patients with HIV. *AJNR. Am. J. Neuroradiol.* 27 (3), 656–66016552012.
- Wu, Y., et al., 2008. Whole brain and localized magnetization transfer measurements are associated with cognitive impairment in patients infected with human immunodeficiency virus. *AJNR. Am. J. Neuroradiol.* 29 (1), 140–145. <http://dx.doi.org/10.3174/ajnr.A074017928382>.
- Yoshizawa, T., Motonishi, S., Saitoh, M., 2007. [Case of acute primary HIV infection with meningoencephalitis demonstrating high signal intensity of the bilateral globus pallidus in T2-weighted MRI]. *Rinsho Shinkeigaku* 47 (9), 597–60018018620.